energies

MDPI

Article

Enhanced Pool Boiling Heat Transfer on Hybrid Wettability Downward-Facing Surfaces: Impact of Interfacial Phenomena and Rewetting Characteristics

Xiaojia Li, Qingyun Long, Jingtao Xue, Zhiguang Liang, Binghuo Yan and Laishun Wang *

Sino-French Institute of Nuclear Engineering and Technology, Sun Yat-Sen University, Zhuhai 519082, China; lixj289@mail2.sysu.edu.cn (X.L.); longqy7@mail2.sysu.edu.cn (Q.L.); xuejt3@mail2.sysu.edu.cn (J.X.); liangzhg5@mail2.sysu.edu.cn (Z.L.); yanbh3@mail.sysu.edu.cn (B.Y.)

* Correspondence: wanglaish@mail.sysu.edu.cn

Abstract: The nucleation and growth of bubbles on homogeneous wetting surfaces have been extensively studied, but the intricate dynamics on hybrid wetting surfaces remain under-explored. This research aims to elucidate the impact of hybrid wettability on pool boiling heat transfer efficiency, specifically under downward-facing heating conditions. To this end, a series of hybrid wettability surfaces with varying hydrophilic and hydrophobic configurations are meticulously fabricated and analyzed. The study reveals distinctive interfacial phenomena occurring at the boundary between hydrophilic and hydrophobic regions during the boiling process. Experimental results indicate that surfaces with a higher proportion of hydrophilic to hydrophobic interfaces exhibit reduced superheat requirements and enhanced boiling heat transfer coefficients for equivalent heat flux densities. Furthermore, the rewetting characteristics of hybrid wettability surfaces are identified as pivotal factors in determining their critical heat flux (CHF). This investigation underscores the potential of hybrid wettability surfaces to optimize pool boiling heat transfer, offering valuable insights for the design and en-hancement of heat exchangers and other thermal management systems.

Keywords: hybrid wettability; pool boiling; CHF

Citation: Li, X.; Long, Q.; Xue, J.; Liang, Z.; Yan, B.; Wang, L. Enhanced Pool Boiling Heat Transfer on Hybrid Wettability Downward-Facing Surfaces: Impact of Interfacial Phenomena and Rewetting Characteristics. *Energies* **2024**, *17*, 5849. https://doi.org/10.3390/en17235849

Academic Editor: Francesco Nocera

Received: 7 August 2024
Revised: 23 August 2024
Accepted: 28 August 2024
Published: 22 November 2024

1. Introduction

A multitude of studies have corroborated that the angular positioning of the heating interface significantly influences boiling heat transfer by altering bubble dynamics upon said interface. Observations suggest that a thicker thermal boundary layer, in tandem with an increased density of nucleation sites, propitiates bubble coalescence [1], thereby engendering sizable vapor formations even in the regime of low thermal flux. The work of Theofanous et al., Rouge et al., Cheung et al., and Hsu et al. has shed light on the fact that the CHF on surfaces facing downward is inextricably linked to the localized mass flow instigated by natural convection. This is inherently governed by geometric determinants such as the orientation of the gravitational vector relative to the surface and the geometrical configuration of the heating element [2–4]. Upon inclined heating substrates, bubbles exhibit migration congruent with the incline trajectory. Nonetheless, when compared to substrates with pronounced inclination, surfaces oriented horizontally and downward impede the liquid wetting process due to a pronounced bubble aggregation effect, leading to the lowest CHF amongst various examined inclinations [5]. Consequently, the quest to enhance both the critical heat flux and the boiling heat transfer coefficient in these specific circumstances has become an area of considerable interest within the research community.

Hydrophilic surfaces enhance CHF but compromise heat transfer. Conversely, hydrophobic surfaces increase the boiling heat transfer coefficient due to higher bubble nucleation rates, yet they reduce CHF [6,7]. Thus, surfaces with composite wetting properties, merging hydrophilic and hydrophobic characteristics, have begun to attract attention.

Betz et al. [8] created surfaces with distinct hydrophobic or hydrophilic domains, finding that surfaces with mixed wettability demonstrated a 65% higher CHF and a 100% increased heat transfer coefficient than conventional hydrophilic surfaces, with similar results from patterns mixing super-hydrophilic and super-hydrophobic features. Hsu's comparative analysis on surface wettability revealed that the contact angle difference between hydrophobic and hydrophilic zones is a key factor in pool boiling [9]. Hsu et al. [10] modified copper surfaces to create varying ratios of hydrophilic and hydrophobic areas, determining that bubble dynamics on these surfaces significantly affect nucleate boiling behavior. Liang et al. [11] prepared surfaces on copper with mixed wettability using dot and stripe patterns. The study findings revealed that surfaces with a dot pattern exhibited a higher CHF and heat transfer coefficient compared to surfaces with a stripe pattern. The value of CHF for the mixed wettability surface was found to be directly proportional to the proportion of the pattern area in relation to the total surface area. C.S. et al. [12] conducted a comparative analysis to evaluate the impact of wettability differences and square hydrophobic coatings on boiling heat transfer. This was achieved by printing hydrophobic coatings on various hydrophilic surfaces. The results demonstrated a leftward shift in the boiling curves on surfaces with non-uniform wetting, leading to an increase in the boiling heat transfer coefficient. Furthermore, an increase in the hydrophobic surface on the copper surface resulted in the shortest bubble detachment time. Chen et al. [13] observed and analyzed the behavior of bubbles on hydrophilic and hydrophobic surfaces, highlighting that the enhanced heat transfer mechanism on these surfaces involved an increase in nucleation sites and a decrease in bubble diameter. The increase in CHF was attributed to the delayed formation of vapor film.

Many researchers have conducted numerical simulations to study the boiling performance of mixed wettability surfaces. Gong et al. [14] utilized the lattice Boltzmann method to simulate mixed wettability surfaces and found that the size of the CHF could be influenced by adjusting the vapor diffusion behavior on the heating surface through the modulation of the hydrophobic area. Yu et al. [15] developed a three-dimensional model using the lattice Boltzmann method and incorporated hydrophobic square pillars on hydrophilic walls. The study determined that the optimal contact angle in the hydrophilic region decreased as the wall superheat increased. Li et al. [16] employed a molecular dynamics simulation to investigate boiling phenomena on mixed wettability surfaces. The research findings indicated that at lower degrees of superheat, nucleation occurred earlier on hydrophobic walls with partially hydrophilic regions compared to purely hydrophobic surfaces.

The majority of previous research on non-uniform hybrid wettability has focused on scenarios where the heating surface is oriented horizontally upward. Observations indicate that when the heating surface is oriented horizontally downward, merged bubbles are prone to blanket the surface, which hampers their detachment from the wall and leads to a substantial divergence in behavior compared to upward-facing conditions. This particular orientation has been insufficiently investigated in the existing literature. Consequently, this paper endeavors to elucidate the influence of hybrid wettability on boiling heat transfer under the condition that the heating surface is horizontally downward-facing.

2. Experimental Section

Detailed descriptions of the experimental setup were reported in publications of our group (e.g., [17]). Hence, only a brief overview will be presented here. The apparatus comprises several components, including a transparent water tank, test section, a preheater, an adjustable height bracket, and a high-speed camera. To heat the water within the tank to its saturation temperature, electric heating rods were installed. Figure 1 provides a schematic diagram of the experimental head made of stainless steel. Silver soldering was employed to join stainless steel metal sheets with a copper heating block, safeguarding against the melting of the sealing silicone and insulation layer when exposed to high heat flux. Three K-type thermocouples, each with an accuracy of 0.1% and a diameter of 0.6 mm,

were positioned along the centerline at the bottom of the copper block. The thermocouples were spaced 3 mm apart, with the bottom thermocouple located 1 mm from the copper surface. An insulation layer was then applied externally to ensure measurement accuracy. The boiling surface temperature can be obtained using the linear extrapolation method. The insulation layer, composed of polyether ether ketone (PEEK) material, was utilized. Given the presence of the insulation layer, we can confidently disregard any potential transverse heat dissipation. The surface of the test section was 2.4 cm × 2.4 cm. During the experimentation, a stepped heating method was employed. The transformer voltage was increased once the thermocouple temperature ceased to change. A higher power increase was applied in the initial stage, while a smaller power increase was used as it approached the CHF. As the voltage applied to the heater increased, the temperatures recorded by the three thermocouples exhibited a sudden and significant rise, indicating that the heat flux at that moment exceeded the CHF threshold (increased by more than 10 °C within 5 s). The heat flux value under the previous stable condition was regarded as the CHF value for that specific step. In accordance with the one-dimensional steady-state Fourier thermal conduction law, the surface temperature of the stainless steel could be determined:

$$T_{wall} = T_1 - q'' \left(\frac{\delta_{Cu}}{k_{Cu}} + \frac{\delta_{Ag}}{k_{Ag}} + \frac{\delta_{Fe}}{k_{Fe}} \right) \tag{1}$$

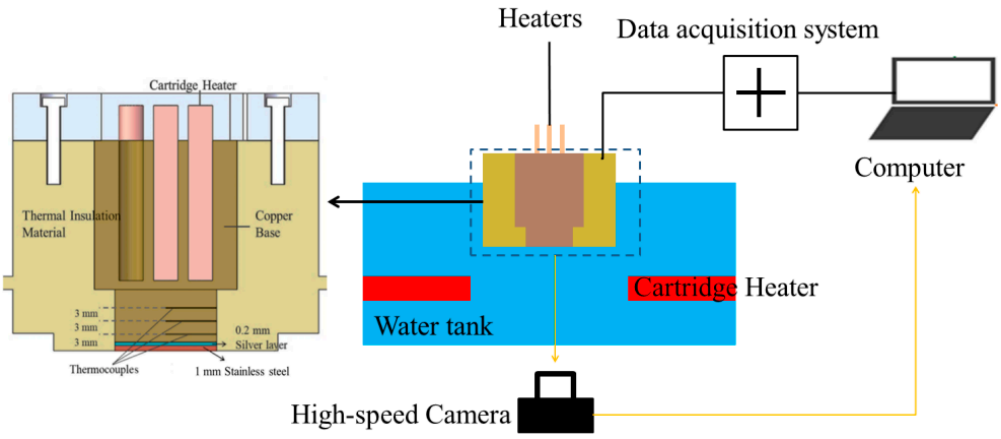

Figure 1. Schematic diagram of pool boiling experimental facility.

This study involved calculating the heat flux rate q'', the degree of superheating (ΔT), and the heat transfer coefficient (h). The least-squares method was employed to derive an optimal linear curve for temperature data and the distance interval. The slope (dT/dx) obtained from this curve was then multiplied by the thermal conductivity (k) to determine q'' and h:

$$q'' = k\frac{dT}{dx} \tag{2}$$

$$h = \frac{q''}{dT} \tag{3}$$

And the standard deviations $\sigma q''$, $\sigma(\Delta T)$, and σh are given by the following equations:

$$\sigma q'' = \sqrt{\frac{s^2 n}{\sigma}} \tag{4}$$

$$\sigma(\Delta T) = \sqrt{\frac{s^2 \sum T_i^2}{\sigma}} \tag{5}$$

$$\sigma h = \sqrt{\left(\frac{\partial h}{\partial(\Delta T)} \sigma(\Delta T) \right)^2 + \left(\frac{\partial h}{\partial q} \sigma q'' \right)^2} \tag{6}$$

$$s = \sqrt{\frac{1}{n-2}\sum(y_i - (bx_i + a))^2} \tag{7}$$

$$\sigma = n\sum {x_i}^2 - \left(\sum x_i\right)^2 \tag{8}$$

$$RSS = \sum_{i=1}^{n}\left[\lg(q_{CHF,Pred,i}) - \lg\left(q_{CHF,Exp,i}\right)\right]^2 \tag{9}$$

$$ACD = 1 - \left(1 - R^2\right)\frac{n-1}{n-m-1} \tag{10}$$

$$MAD = \frac{1}{n}\sum_{i=1}^{n}|RD_i| \tag{11}$$

where

$$RD = \frac{q_{CHF,Pred} - q_{CHF,Exp}}{q_{CHF,Exp}} \tag{12}$$

$$R^2 = 1 - \frac{\sum_{i=1}^{n}\left[\lg(q_{CHF,Pred,i}) - \lg\left(q_{CHF,Exp,i}\right)\right]^2}{\sum_{i=1}^{n}\left[\lg(q_{CHF,Pred,i}) - \lg\left(\frac{1}{n}\sum_{i=1}^{n} q_{CHF,Exp,i}\right)\right]^2} \tag{13}$$

In this context, T_i (y_i) is the temperature at location i, x_i is the distance interval relative to the boiling surface, k is the thermal conductivity, and n is the number of temperature measurement points (3 thermocouple positions). The maximum uncertainty in each instance did not exceed 10%.

In order to fabricate surfaces with hybrid wettability, the removal of surface contaminants was carried out by polishing with #2000 grit sandpaper. Subsequently, a sequential triple-rinsing process was employed, wherein acetone, ethanol, and deionized water were utilized in a sequential manner to achieve a clean stainless steel substrate. The preparation of surfaces with hybrid wettability was accomplished through the utilization of a sol–gel method, which is elaborated upon in the following sections:

Initially, solution A was synthesized by reacting tetraethyl orthosilicate (TEOS) with deionized water using a molar ratio of 1:4. In parallel, solution B was formulated by mixing ethanol with deionized water in a molar ratio of 1:3. Thereafter, these two solutions were blended at a volume ratio varying from 1.5 to 100, to which SiO_2 nanoparticles with a diameter of 40 nm were added. The resulting mixture was subjected to magnetic stirring at ambient temperature for a duration of one hour. High-temperature-resistant tape was then precisely applied to the stainless steel substrate to establish defined hydrophilic boundaries, and the stirred mixture was subsequently deployed onto the prepared heating surface. The tape was instrumental in maintaining a sharp distinction between the hydrophilic zones and the unmodified stainless steel substrate. The finalization of the procedure involved baking the treated surface at 180 °C for a period of 90 min, followed by a gradual return to ambient temperature. Upon removal of the tape, a surface with designated regions of hybrid wettability was unveiled.

In the present study, surfaces were engineered to exhibit varying degrees of hybrid wettability, as delineated in Figure 2, wherein the hydrophilic region uniformly constituted 50% of the total surface area. The contact angle of the untreated surface was 86°, and the contact angle of the hydrophilic surface was 21.2°. The thickness of the hydrophilic layer was 3.74 μm. The designs varied in the distribution and orientation of hydrophilic and hydrophobic interfaces, exemplified by surface specimens #2 and #3 which presented reciprocal arrangements of the hydrophilic and hydrophobic domains. After the experiment, the contact angle of the hydrophilic surface was measured, and it was observed that there was no significant change in the contact angle.

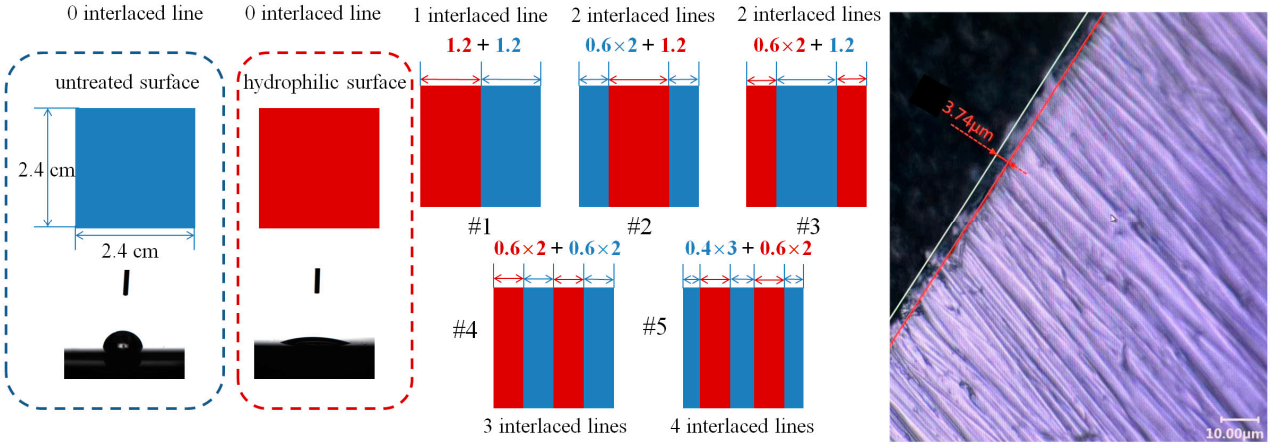

Figure 2. List of the surface types and corresponding parameters.

3. Experimental Results and Analysis

3.1. Hybrid Wettability Surface Boiling Heat Transfer

Figure 3a depicts the evolution of bubble growth on stainless steel surfaces subjected to varying heat flux densities. With the continuous increase in heat flux, the bubbles are observed to progressively enlarge. Upon reaching a critical size, the bubbles coalesce to form larger entities. Owing to the downward orientation of the heating face, buoyancy does not facilitate the detachment of bubbles from the surface; rather, the bubbles continue to expand, culminating in the development of a vapor film that encases the heating surface. As additional bubbles amalgamate, the size of the vapor film increases, until steam generation induces the film to ascend away from the heating surface. Figure 3b illustrates the growth state of bubbles on a hydrophilic surface at varying heat flux densities. It can be observed that the bubbles developing on the surface are more sparsely distributed. As bubbles on the surface coalesce and increase in size, the departure of bubbles results in a swift replenishment of water to the wall.

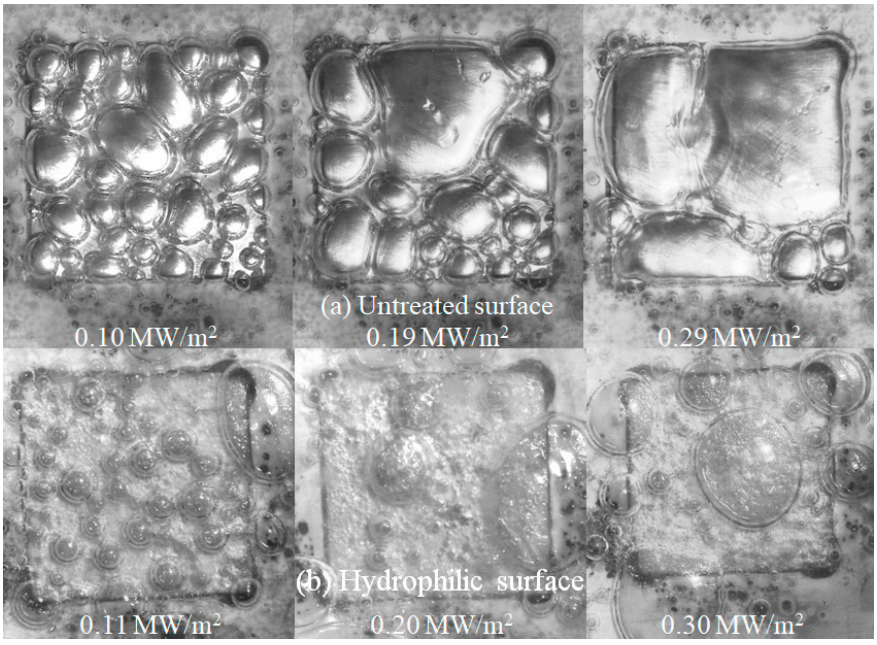

Figure 3. Nucleation conditions under different heat flux densities on different surfaces.

The critical heat flux can be interpreted as the outcome of a competition between two distinct rates: the rate of bubble expansion and detachment from the wall due to

heating, and the rate at which the surrounding fluid restores the liquid layer. When the liquid replenishment rate is sufficient to rapidly replace the liquid post bubble departure, uninterrupted heat removal can be sustained. In contrast, at elevated temperatures, when the rate of bubble production surpasses the liquid replenishment rate, the liquid's inability to uniformly coat the heating surface gives rise to film boiling. Hydrophilic surfaces, characterized by their robust water-absorbing properties, facilitate expedited fluid replenishment around the heated and coalesced bubbles compared to untreated surfaces, thus enhancing heat transfer capacity at maintained heat flux densities and consequently demonstrating a superior CHF.

The dynamics of the governing bubble motion on hybrid wettability surfaces are considerably more intricate than those observed on homogeneous wettable surfaces. Figure 4 illustrates the behavior of bubbles on surface #1, with the left section being hydrophilic and the right section untreated. Observations reveal that, on the untreated segment, a film forms over the surface subsequent to bubble coalescence. Conversely, on the hydrophilic segment, bubbles coalesce and increase in size before merging with those on the untreated segment, after which the hydrophilic surface becomes re-covered by liquid. Thereafter, a persistent vapor film overlays the untreated segment, with heat dissipation occurring predominantly through the hydrophilic section. As the heat flux continues to escalate, bubbles on the hydrophilic section enlarge progressively until a vapor film extends across the entire heating surface.

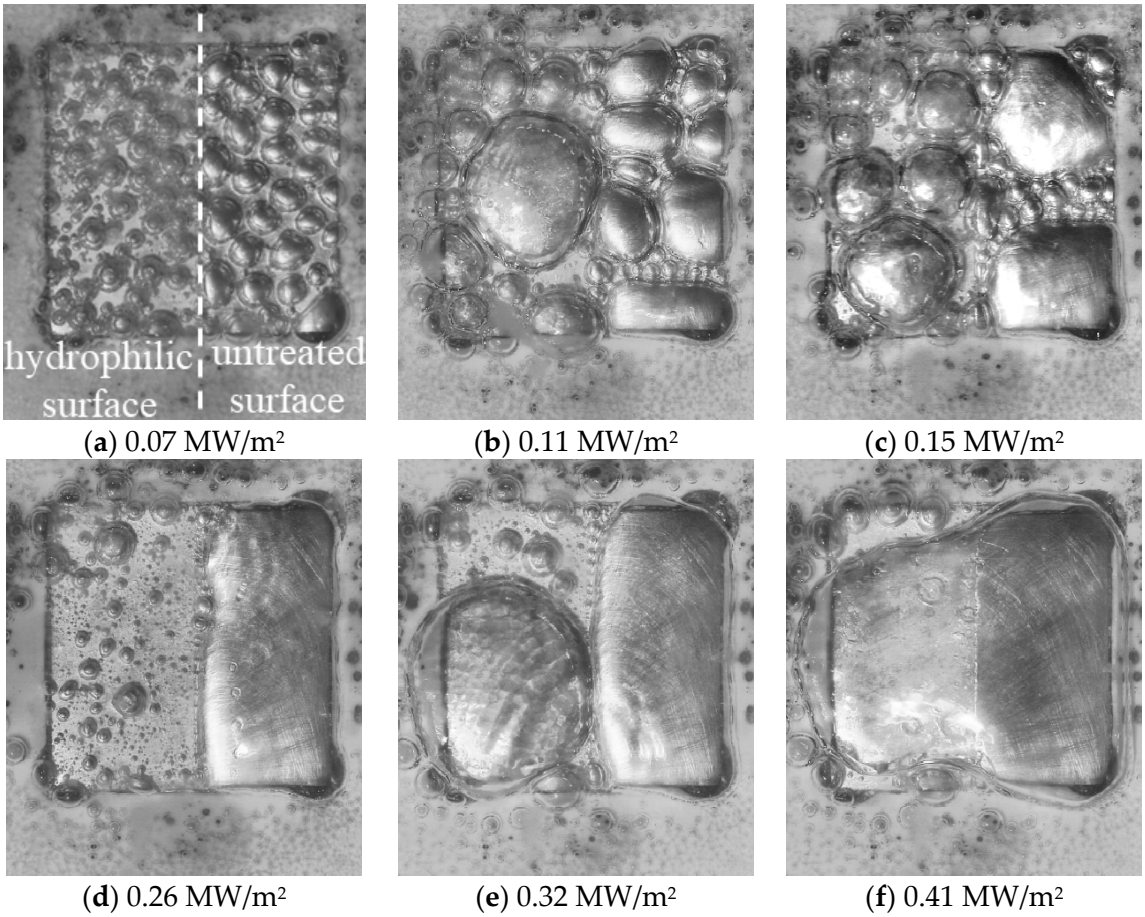

(**a**) 0.07 MW/m^2 (**b**) 0.11 MW/m^2 (**c**) 0.15 MW/m^2

(**d**) 0.26 MW/m^2 (**e**) 0.32 MW/m^2 (**f**) 0.41 MW/m^2

Figure 4. The behavior of bubbles on surface #1.

Figure 5 displays photographs of water resupply after bubble detachment on different surfaces under the same heat flux, where a noticeable difference is observed: in (b,c), the edges are hydrophilic surfaces and water replenishes from both sides; in (d,e), the edges are untreated surfaces and the replenishing water forms a crescent-shaped gas–liquid interface.

This is attributed to water spreading rapidly on hydrophilic surfaces, while it spreads more slowly on untreated surfaces, thus creating a velocity difference and leading to the curved gas–liquid interface.

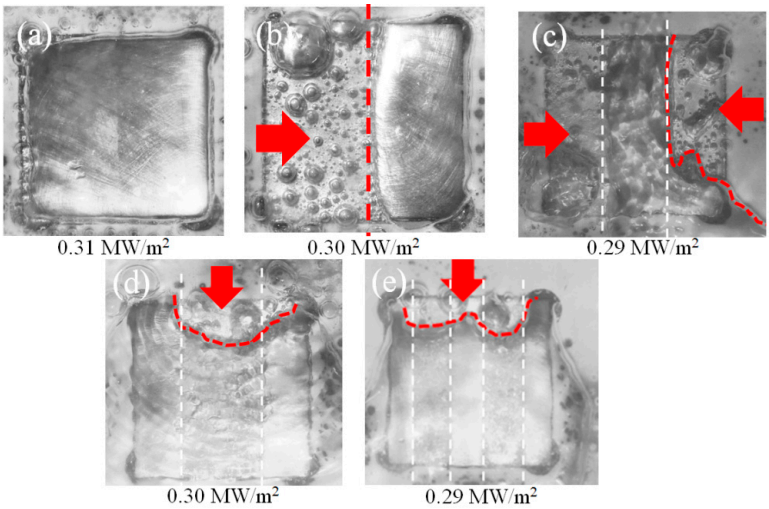

Figure 5. Snapshots of rewetting after bubble detachment on different surfaces. (**a**) Surface #1, (**b**) #2, (**c**) #3, (**d**) #4, and (**e**) #5.

Thus, the differences in surface wettability reflect that hydrophilic surfaces rapidly absorb water, whereas untreated surfaces rehydrate more slowly. This is because varying hydrophilic–hydrophobic patterns result in different rehydration rates after bubbles detach from the surface.

Figure 6a presents the variation in critical heat flux for various hydrophilic and hydrophobic surfaces under different heat flux densities. As depicted, Surface #3 exhibits the highest CHF, followed by the hydrophilic surfaces #1, #2, #4, and #5, respectively. Notably, the untreated surface demonstrates the lowest CHF. Among these surfaces, the addition of a hydrophilic coating consistently enhances the CHF, albeit to varying extents. However, the CHF values differ among the hydrophilic surfaces due to their identical area and differing configurations. Figure 6b presents the variation in the boiling heat transfer coefficient over time during the boiling process. It is observable that the hydrophilic–hydrophobic interface has a significant effect on the heat transfer coefficient. For surfaces without such interfaces, the hydrophilic surface exhibits the lowest heat transfer coefficient, while the untreated surface has a slightly higher coefficient. As the number of interfaces increases, the heat transfer coefficient continues to rise. This increase is due to bubble-induced agitation enhancing the fluid flow in pool boiling heat transfer, which in turn elevates the heat transfer coefficient. The hydrophilic surface's stronger attraction to water molecules makes it harder for them to detach from the surface, requiring more energy for nucleation, thus making nucleation more difficult, resulting in a lower bubble density on hydrophilic surfaces obstructing the heat transfer. On hydrophobic surfaces, less energy is required for nucleation, leading to a higher density of bubbles and therefore, a higher heat transfer coefficient compared to hydrophilic surfaces. At the same temperature, bubbles are more likely to form on the interfaces between hydrophilic and hydrophobic areas, which means surfaces with hydrophilic–hydrophobic interfaces have a stronger heat transfer capability than those without them, and this capability further increases with the number of interfaces.

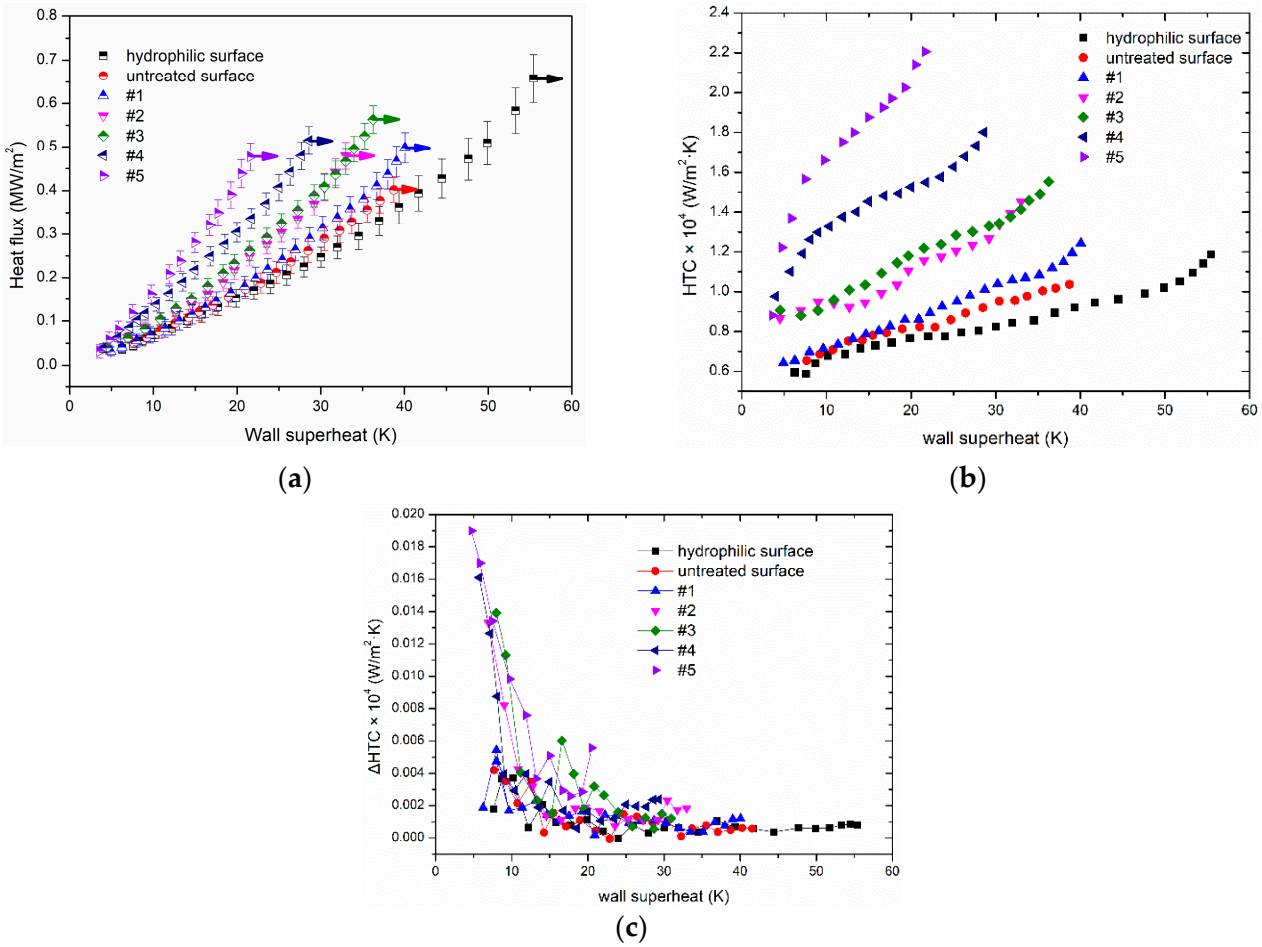

Figure 6. Boiling curves on different surfaces. (**a**) Boiling heat transfer curve; (**b**) boiling heat transfer coefficient variation curve with superheat degree; and (**c**) boiling heat transfer coefficient increment curve with superheat degree.

Upon comparing Figure 6a,b, an inverse relationship is discerned between the heat transfer coefficients of the surfaces and their corresponding degrees of superheat at equivalent heat flux densities. This observation implies that surfaces endowed with a greater quantity of hydrophilic–hydrophobic junctions successfully sustain reduced temperatures when subjected to the same heat flux, which concurrently contributes to the preservation of the surface material. Figure 6c presents the dynamic behavior of the incremental heat transfer coefficient for a variety of surfaces in relation to changing degrees of superheat throughout the heat transfer process. It is noted that surfaces with hydrophilic–hydrophobic interfaces exhibit a pronounced augmentation in the increment of the heat transfer coefficient at reduced superheat, which subsequently diminishes with the increment of superheat. Initially, as boiling commences, the heat transfer coefficient is relatively low; however, it reaches a peak with the rapid nucleation and growth of bubbles at the interfaces. As the bubble population approaches a state of equilibrium, the elevation in the heat transfer coefficient correspondingly reduces and achieves stability. In stark contrast, surfaces devoid of such interfaces demonstrate a relatively constant incremental heat transfer. Moreover, for surfaces with hydrophilic–hydrophobic junctions, it is observed that with an increase in the density of hydrophilic–hydrophobic strip patterns, there is a concurrent rise in the heat transfer coefficient increment during the early stage of boiling. This phenomenon can be ascribed to the fact that a higher count of hydrophilic–hydrophobic interfaces correlates with an intensified bubbling activity, thereby significantly enhancing the heat transfer coefficient increment in the initial boiling period.

3.2. Prediction of Surface-Down Pool Boiling CHF Relation

During the experimental observations, it was discerned that in proximity to the CHF condition, the hydrophilic regions of the surface exhibited an enhanced wicking capability, which facilitated a more rapid rehydration process compared to the untreated surfaces, thus promoting continual heat transfer and postponing the CHF. However, in this study's hybrid wettability wall, the hydrophilic ratio was maintained at 50%, yet there were significant differences in CHF, attributable to the different hydrophilic–hydrophobic patterns. To further investigate the influence of these patterns on the CHF, wettability assessments were conducted on various surfaces. The phenomena captured in Figure 5 elucidate that during the boiling process, the water absorption is predominantly facilitated by hydrophilic surfaces, whereas untreated surfaces tend to be largely occluded by vapor bubbles, thereby hindering any substantial water repletion or surface wetting from the adjacent liquid. In light of this, the hydrophilic surfaces play an indispensable role in mitigating issues related to water replenishment.

Figure 7 shows that different surfaces possess diverse hydrophilic shapes, thus resulting in varying water replenishment behaviors. It is necessary to calculate the water absorption area for the different surfaces. Since the drop spreading rate on the untreated surfaces is almost negligible when compared to that on the hydrophilic surfaces, only the replenishing area for the hydrophilic surfaces needs to be considered.

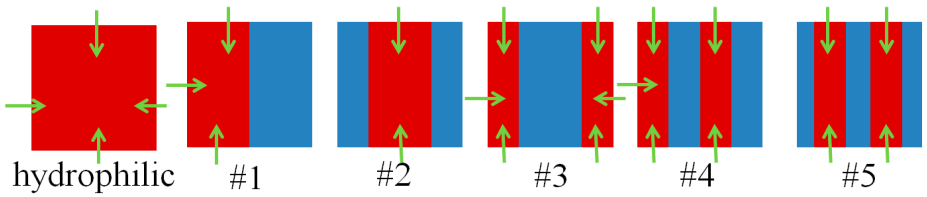

Figure 7. Direction of liquid replenishment when rewetting different surfaces.

Zuber [18] constructed a CHF model by analyzing the Tayler wave and Helmhotz instability:

$$q''_{CHF} = 0.131\rho_g^{0.5} h_{lg} \left[\sigma g(\rho_l - \rho_g)\right]^{0.25} \tag{14}$$

On this basis, El-Genk and Guo [19] provided the formula for heat flux on a downward-facing (0°) heated surface:

$$q''_{CHF} = 0.1455\rho_g^{0.5} h_{lg} \left[\sigma g(\rho_l - \rho_g)\right]^{0.25} \tag{15}$$

In this study, the correlation for downward-facing CHF based on the Zuber model is also proposed:

$$q''_{CHF} = 0.1455\rho_g^{0.5} h_{lg} \left[\sigma g(\rho_l - \rho_g)\right]^{0.25} \left(C_1 + C_2 \cdot s + C_3 \cdot s^2\right) \tag{16}$$

where C_1, C_2, and C_3 are constants to be determined and s represents the dimensionless number signifying the proportion of the rewetted area to the total surface area, which is the ratio of the surface rewet area to the total area.

Compared to (10), the relationship proposed in (11) considers the influence of the rewetting ability on CHF. In the first part of Equation (11), the correlation $0.1455\rho_g^{0.5} h_{lg} \left[\sigma g(\rho_l - \rho_g)\right]^{0.25}$ is similar to that of Zuber, El-Genk, and Guo, while the correlation $\left(C_1 + C_2 \cdot s + C_3 \cdot s^2\right)$ in the second part incorporates the effects of different mixed surfaces on CHF by introducing the surface rewetting capability.

Tables 1 and 2 showcase the static parameters and analysis results. The residual sum of squares (RSS) and the adjusted coefficient of determination (ACD) can be calculated using Equations (9) and (10), respectively. Furthermore, the mean absolute deviation

(MAD) provides a measure of the average prediction accuracy, which can be obtained using Equation (11).

Table 1. Analysis results of the new correlation.

Constant	Value	Standard Error
C_1	0.4014	0
C_2	0.16341	0.01612
C_3	0.13194	0.02269

Table 2. Statistics parameters of the new correlation.

Statistics Parameters	Value
Number of points	7
Degrees of freedom	6
Residual sum of squares	0.01265
Adjusted coefficient of determination	0.99344

Thus, Equation (11) can be rewritten as

$$q''_{CHF} = q''_{CHF} = 0.1455\rho_g^{0.5} h_{lg} [\sigma g(\rho_l - \rho_g)]^{0.25} \left(0.4014 + 0.16341 \cdot s + 0.13194 \cdot s^2\right) \quad (17)$$

In this study, a 100% prediction rate within ±10% was achieved for the entire database, indicating a strong correlation. The calculation of the residual sum of squares (RSS) and the mean absolute deviation (MAD) yielded values of 0.01265 and 2.4%, respectively, when comparing the predicted and experimental CHF values. These findings, illustrated in Figure 8, highlight the excellent agreement between the predicted values and the measured data. The CHF prediction model established in this paper can serve as a reference for predicting outcomes on surfaces with hybrid wettability.

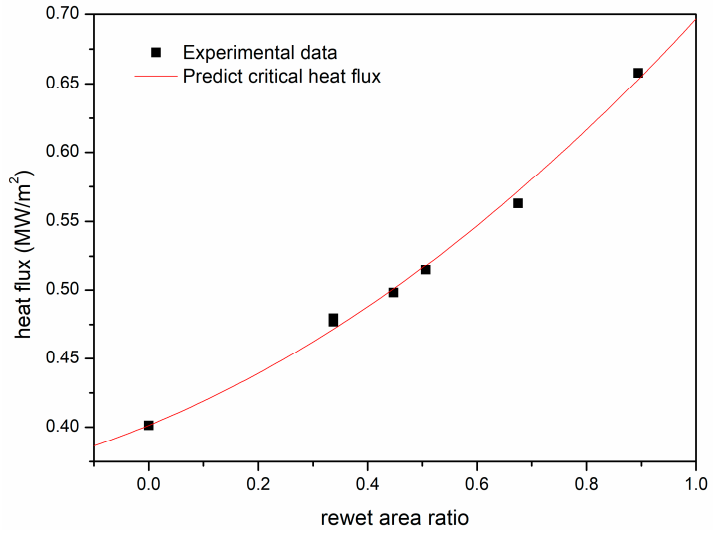

Figure 8. Comparison between predicted critical heat fluxes and experimental data.

4. Conclusions

In this study, we examine the effects of hybrid wettability surfaces on pool boiling heat transfer for downward-facing heating. We prepared surfaces with hybrid wettability and employed experimental methods to compare the boiling behavior on surfaces with different configurations. The main research findings and conclusions can be summarized as follows:

1. Prior to nucleation, surfaces with hydrophilic characteristics demonstrate enhanced heat transfer efficiency, while their hydrophobic counterparts require less energy to initiate nucleation. However, hybrid wettability surfaces combine the advantages of both, resulting in higher heat transfer efficiency. Surfaces with a larger number of hydrophilic–hydrophobic interfaces exhibit superior heat transfer performance.
2. The variation in critical heat flux (CHF) among hybrid wettability surfaces of different shapes is attributed to differences in the rewetting capability. Surfaces with hydrophilic areas located closer to the edges exhibit a stronger rewetting capability, leading to higher CHF values.
3. A predictive model for the CHF of hybrid wettability surfaces, based on the rewetted area, has been formulated. Experimental data confirm that the results closely align with the model's predictions.

Author Contributions: Conceptualization, L.W. and B.Y.; Methodology, X.L.; Software, X.L.; Validation, Q.L.; Formal analysis, J.X. and Z.L.; Investigation, J.X.; Writing—original draft, X.L.; Writing—review & editing, L.W.; Visualization, Q.L.; Supervision, Z.L. and B.Y.; Funding acquisition, L.W. All authors have read and agreed to the published version of the manuscript.

Funding: This research was financially supported by the National Natural Science Foundation of China (No. 12005318).

Data Availability Statement: Data are contained within the article.

Conflicts of Interest: The authors declare that they have no known competing financial interests or personal relationships that could have appeared to influence the work reported in this paper. All authors have read and agreed to the published version of the manuscript.

References

1. Hsu, Y.Y. On the size range of active nucleation cavities on a heating surface. *J. Heat Transf.* **1962**, *84*, 207–213. [CrossRef]
2. Theofanous, T.; Syri, S.; Salmassi, T.; Kymäläinen, O.; Tuomisto, H. Critical heat flux through curved, downward facing, thick walls. *Nucl. Eng. Des.* **1994**, *151*, 247–258. [CrossRef]
3. Rouge, S. SULTAN test facility for large-scale vessel coolability in natural convection at low pressure. *Nucl. Eng. Des.* **1997**, *169*, 185–195. [CrossRef]
4. Cheung, F.; Haddad, K. A hydrodynamic critical heat flux model for saturated pool boiling on a downward facing curved heating surface. *Int. J. Heat Mass Transf.* **1997**, *40*, 1291–1302. [CrossRef]
5. Ohtake, H.; Koizumi, Y. Engineering, Study on ex-vessel cooling of reactor pressure vessel (model analysis of critical heat flux on inclined plate and hemisphere facing downward). *JSME Int. J. Ser. B* **2004**, *47*, 351–357. [CrossRef]
6. Jo, H.; Ahn, H.S.; Kang, S.; Kim, M.H. A study of nucleate boiling heat transfer on hydrophilic, hydrophobic and heterogeneous wetting surfaces. *Int. J. Heat Mass Transf.* **2011**, *54*, 5643–5652. [CrossRef]
7. Jo, H.J.; Kim, H.; Ahn, H.S.; Kim, S.; Kang, S.H.; Kim, J.; Kim, M.H. Experimental study of boiling phenomena by micro/milli hydrophobic dot on the silicon surface in pool boiling. In Proceedings of the International Conference on Nanochannels, Microchannels, and Minichannels, Pohang, Republic of Korea, 22–24 June 2009; pp. 93–97.
8. Betz, A.R.; Jenkins, J.; Attinger, D. Boiling heat transfer on superhydrophilic, superhydrophobic, and superbiphilic surfaces. *Int. J. Heat Mass Transf.* **2013**, *57*, 733–741. [CrossRef]
9. Hsu, C.C.; Chiu, W.C.; Kuo, L.S.; Chen, P.H. Reversed boiling curve phenomenon on surfaces with interlaced wettability. *AIP Adv.* **2014**, *4*, 107110. [CrossRef]
10. Hsu, C.-C.; Lee, M.-R.; Wu, C.-H.; Chen, P.-H. Effect of interlaced wettability on horizontal copper cylinders in nucleate pool boiling. *Appl. Therm. Eng.* **2017**, *112*, 1187–1194. [CrossRef]
11. Liang, G.; Chen, Y.; Wang, J.; Wang, Z.; Shen, S. Experiments and modeling of boiling heat transfer on hybrid-wettability surfaces. *Int. J. Multiph. Flow* **2021**, *144*, 103810. [CrossRef]
12. Kumar, C.S.; Chang, Y.W.; Chen, P.H. Effect of heterogeneous wettable structures on pool boiling performance of cylindrical copper surfaces. *Appl. Therm. Eng.* **2017**, *127*, 1184–1193. [CrossRef]
13. Chen, X.; Qiu, H. Bubble dynamics and heat transfer on a wettability patterned surface. *Int. J. Heat Mass Transf.* **2015**, *88*, 544–551. [CrossRef]
14. Gong, S.; Cheng, P. Numerical simulation of pool boiling heat transfer on smooth surfaces with mixed wettability by lattice Boltzmann method. *Int. J. Heat Mass Transf.* **2015**, *80*, 206–216. [CrossRef]
15. Yu, Y.; Wen, Z.; Li, Q.; Zhou, P.; Yan, H. Boiling heat transfer on hydrophilic-hydrophobic mixed surfaces: A 3D lattice Boltzmann study. *Appl. Therm. Eng.* **2018**, *142*, 846–854. [CrossRef]

16. Li, X.; Ming, P.; Yu, G.; Chen, Y.; Tan, Z.; Ma, Y. The influence of cone structure and wettability on vaporization nucleation. *J. Mol. Liq.* **2023**, *390*, 123080. [CrossRef]
17. Wang, L.; Ye, W.; He, X.; Wu, S.; Ming, P.; Wang, J.; Cheng, H.; Yan, B. Experimental study on the CHF enhancement effect of nanofluids on the oxidized low carbon steel surface, Applied Thermal Engineering. *Appl. Therm. Eng.* **2022**, *204*, 117968. [CrossRef]
18. Zuber, N. Hydrodynamic Aspects of Boiling Heat Transfer. Ph.D. Thesis, University of California, Los Angeles, CA, USA, 1959.
19. El-Genk, M.S.; Guo, Z. Transient boiling from inclined and downward-facing surfaces in a saturated pool. *Int. J. Refrig.* **1993**, *16*, 414–422. [CrossRef]